

Nonlinear dynamics and failure wind velocity analysis of urban trees

Xiaoqiu Ai¹, Yingyao Cheng¹ and Yongbo Peng^{*1,2}

¹Shanghai Institute of Disaster Prevention and Relief, Tongji University, China

²State Key Laboratory of Disaster Reduction in Civil Engineering, Tongji University, China

(Received June 30, 2015, Revised October 27, 2015, Accepted October 28, 2015)

Abstract. With an aim to assess the wind damage to urban trees in more realistic conditions, the nonlinear dynamics of structured trees subjected to strong winds with different levels is investigated in the present paper. For the logical treatment of dynamical behavior of trees, material nonlinearities of green wood associated with tree biomechanics and geometric nonlinearity of tree configuration are included. Applying simulated fluctuating wind velocity to the numerical model, the dynamical behavior of the structured tree is explored. A comparative study against the linear dynamics analysis usually involved in the previous researches is carried out. The failure wind velocity of urban trees is then defined, whereby the failure percentages of the tree components are exposed. Numerical investigations reveal that the nonlinear dynamics analysis of urban trees results in a more accurate solution of wind-induced response than the classical linear dynamics analysis, where the nonlinear effect of the tree behavior gives rise to be strengthened as increasing of the levels of wind velocity, i.e., the amplitude of 10-min mean wind velocity. The study of relationship between the failure percentage and the failure wind velocity provides a new perspective towards the vulnerability assessment of urban trees likely to fail due to wind actions, which is potential to link with the practical engineering.

Keywords: nonlinear dynamics; failure wind velocity; urban trees; geometric nonlinearity; tree biomechanics; wind damage

1. Introduction

The areas affected by hurricanes and cyclones always suffer huge economic losses each year. Amongst these economic losses, a large proportion results from urban storm disasters, of which the wind damage to trees is a main concern for the decision maker of urban planning. In addition, the wind damage to urban trees is one of the factors leading to disruption of transportation routes, power shortages, and surrounding traffic lines (Jim and Liu 1997). As a result, it is necessary to understand the capacity of urban trees with standing in the future storms.

Failure analysis of trees is a challenging issue due to their complex dynamics (Ciftci *et al.* 2014). Over the past decades, a series of research efforts have been made upon this issue. Baker established a theoretical model in function of failure wind velocity, which is suitable for the

*Corresponding author, Associate Professor, E-mail: pengyongbo@tongji.edu.cn

assessment of the wind damage to the trees and crops (Baker 1995). Gardiner and his colleagues provided the empirical models of trees in the forest areas; say ForestGALES and HWIND, to predict the critical wind velocity for tree failure and the probability of this critical wind velocity in even-aged stands (Gardiner *et al.* 2000). Spatz and Speck examined the dynamics of swaying stems of trees induced by winds using a fourth-order partial differential equation (Spatz and Speck 2002). These models show a good applicability in the wind-induced damage of the forest owing to the uprooting and trunk breakage. While very few concerns are laid upon the urban trees (Ciftci *et al.* 2014). Unlike the trees distributed in the forest, the feature of urban trees is typically different. The trees distributed in cities, for example, possess larger crown shapes over those standing in forest so as to meet with the greening requirement of urban planning. With large crown shapes, the trees are liable to the strong wind indicating that wind loads acting on the branches give rise to be significant. Adaptive to the living condition, the branches expose to be longer and heavier than those of the forest trees. The branches, nevertheless, are more vulnerable to break under wind actions. Unfortunately, the specific dynamical behavior of urban trees has not been paid sufficient attentions.

Since the wind-induced damage of urban trees has been an eye-catching event in recent years due to climate change, the tentative studies of urban trees appear. Ciftci *et al.* numerically investigated the structural dynamics of urban trees and derived the failure probability of the trunk taking account of the randomness inherent in the wind action and its effect relevant to seasons (Ciftci *et al.* 2014). It is well acknowledged, however, that the stress-compression curve of green wood exhibits a nonlinear plastic profile with rupture point (Brudi 2002). The failure of the tree thus would not be an all or none process (Spatz and Bruechert 2000). However, most of previous models either represent the dynamics of the plants in their linear elastic range (exposing to be of oscillation of the plants) or employ a Hookean material profile in the definition of the resistance capacity of the tree (Saunderson *et al.* 1999, James 2006, Sellier *et al.* 2008, Dahle and Grabosky 2010, Ciftci *et al.* 2014). Although the assumption of linear dynamics is made in order to simplify the mathematical calculations, the analysis result using the previous models might significantly differ from the real dynamics of trees.

Besides, simplified models of beams or tapered poles were usually used in the numerical analysis of trees in order to reduce the computational cost (Saunderson *et al.* 1999, Spatz and Speck 2002). This treatment, however, would neglect the contribution from the branches to the dynamics of trees (James 2006, Sellier *et al.* 2008, Ciftci *et al.* 2013, Ciftci *et al.* 2014). In recent years, the finite element method (FEM) has been used in the examination of nonlinear dynamical behaviors of trees whereby the geometry nonlinearities associated with the structural motion of branches could be readily included (Sellier *et al.* 2006, 2008, Ciftci *et al.* 2014). Another advantage of the finite element method lies in the capacity to realistically reveal the failure process of the trees through integrating the material nonlinearities and three-dimensional model.

In the next sections, the nonlinear dynamics of an urban tree and its wind-induced damage against failure wind velocity are investigated. The classical weighted amplitude wave superposition (WAWS) method is used for the simulation of fluctuating wind velocity processes, which is detailed in Section 2. Section 3 addresses the nonlinear dynamic model of urban trees employing the finite element method. A comparative study against the linear dynamics analysis usually involved in the previous researches is carried out in Section 4. The failure wind velocity of urban trees is defined in Section 5, whereby the failure percentages of the tree components are exposed. Conclusions are drawn at the final section.

2. Simulation of fluctuating wind velocity

The wind velocity process $U_z(t)$ at a height of z includes two components: the time-averaged component \bar{U}_z and the fluctuating component $u_z(t)$ (Dyrbye and Hansen 1997), i.e.

$$U_z(t) = \bar{U}_z + u_z(t) \quad (1)$$

The time-averaged component \bar{U}_z could be represented by an exponential-type function relevant to the height (Ciftci *et al.* 2014)

$$\bar{U}_z = \bar{U}_h \left(\frac{z}{h}\right)^{1/7} \quad (2)$$

where \bar{U}_h denotes the reference time-averaged component of wind velocity at the reference height h .

The fluctuating wind $u_z(t)$ is typically reviewed as a zero-mean Gaussian process. Several numerical techniques were proposed to simulate the wind fluctuations with an advantage of study on wind-sensitive nonlinear structures, such as the spectral representation approaches and auto-regressive filters method (Kareem 2008). Compared with the auto-regressive filters method, wave superposition based spectral representation schemes can be used in direct simulation of vortex excitation and be proved to guarantee a better simulation (Lipecki and Flaga 2010). The classical weighted amplitude wave superposition method (WAWS) is proved to be high accuracy in the numerical simulation (Rossi *et al.* 2004), though it would be of computational cost in case of the simulation of long-duration multi-variant wind fields (Kareem 2008). With a height-irrelevant hypothesis of fluctuating wind velocity, the WAWS could be readily used in the simulation of wind field of urban trees.

The WAWS operates as a mathematical scheme associated with the power-spectrum-density (PSD) function in the frequency domain (Kareem 2008). Several empirical power-spectral-density functions were proposed and proved to be of applicability for practical engineering, such as the Davenport spectrum (Davenport 1961) and Simiu spectrum (Simiu 1974). With the benefit of the invariant-turbulent-intensity along with the height, the Davenport spectrum; see Eq. (3) is used for the simulation of wind field of urban trees

$$S(f) = 4\kappa\bar{U}_{10}^2 \frac{x^2}{f \left[1 + x^2\right]^{\frac{4}{3}}} \quad (3)$$

$$x = 1200f / \bar{U}_{10}$$

where $S(f)$ denotes the spectral density of the fluctuating wind velocity; f denotes the natural frequency; \bar{U}_{10} denotes the mean wind velocity in time average at the reference height of 10 m; κ denotes the surface drag coefficient, which has the relationship with the roughness length z_0 and the von Karman's constant k as follows (Dyrbye and Hansen 1997)

$$\kappa = \left[\frac{k}{\ln\left(\frac{10}{z_0}\right)} \right]^2 \quad (4)$$

where k is valued by 0.4; z_0 is valued by 1.6 for case of urban area (Dyrbye and Hansen 1997).

The wind fluctuation at height z could be derived through the following equation

$$u_z(t) = \sum_{i=1}^{N_f} H_i(f_i) \cos(2\pi f_{r,i}t + \varphi_i) \quad (5)$$

where $u_z(t)$ denotes the velocity of a time series at the height of z ; N_f denotes the number of frequency internals; $H_i(f_i)$ ($i=1,2,\dots,N_f$) denotes the set of N_f functions which depends upon the frequency interval and the involved power-spectral density-function; f_i ($i=1,2,\dots,N_f$) denotes the central frequency of the i -th frequency interval Δf_i ; $f_{r,i}$ denotes the sum of the i -th central frequency and half of the interval Δf_i ; φ_i denotes the set of N_f random values of phase shift angles, which submits to a uniform distribution and valued from the range 0 to 2π . The details of the WAWS method could refer to the article co-authored by Lipecki and Flaga (2010).

For the investigation of levels of wind strength, six cases of fluctuating wind velocity histories from the mean velocity of 12 m/s to 32 m/s with an interval of 4 m/s for the reference height (10 m above ground) are generated. The spectral density was divided into 20,000 equal parts ($N_f = 20,000$) from 0.00 to 10 Hz in order to obtain a time-history of the stochastic process for a period of 600s. The spectral densities of wind fluctuations at the mean wind velocity of 16 m/s, 20 m/s, and 24 m/s are shown in Fig. 1, respectively. It is noted that the simulated spectrum is in acceptable agreement with the target wind spectrum, indicating that the simulated wind velocity could guarantee a rational calculation of the wind-induced structural response.

3. Modelling of urban trees

A tree, which typically features a complex configuration, consists of branches and leaves. These branches or leaves are different from each other, i.e., no two branches or leaves have the same dimensions or shapes in reality. This fact highlights the variability of trees (James *et al.* 2006), whereby the accurately geometric modelling of trees still remains a challenge. In this study, one of the typical urban trees in China, *Ginkgo*, is examined as the example.

3.1 Geometric modelling

In order to capture the key features of a *Ginkgo* tree's architecture, it is, as a first approximation, typically modelled as a trunk with attachment of primary branches (large branches) and secondary

branches (small branches); see Fig. 2.

In the model, the number of the trunk is 1, while the numbers of the primary and secondary branches (components) are 10, 20, respectively. The spatial curves of the trunk, the primary branches and the secondary branches are constructed through connecting the reference points abstracted from the images of a real tree in spatial coordinates, whereby a virtual *Ginkgo* tree is then established by assembling these curves. The geometry of this *Ginkgo* tree is shown in Fig. 2. The diameter of cross-sectional of trunk at bottom is 0.1 m; the total height of the tree structure is 6m. The cross section along the trunk and branch is ideally assumed to be a solid circle, of which the area at height z is defined as follows

$$A(z) = \pi[R(z)]^2 \tag{6}$$

where $R(z)$ denotes the cross-sectional radius of the trunk at height z , which is relevant to the cross-sectional radius R_0 of the trunk at bottom (Saunderson *et al.* 1999)

$$R(z) = R_0 \left(1 - \frac{z}{H}\right)^\lambda \tag{7}$$

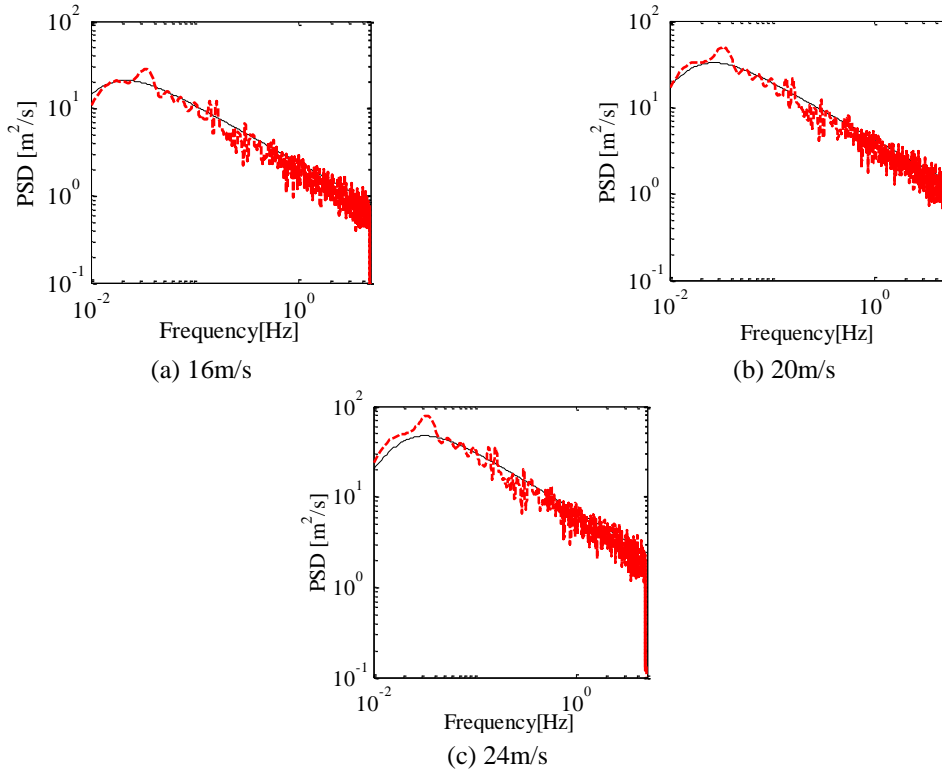


Fig. 1 Wind power spectrum at the mean wind velocity of (a) 16 m/s, (b) 20 m/s and (c) 24 m/s respectively: power spectrum of the simulated wind velocity (dash line); Davenport power spectrum (solid line)

where H denotes the height of tree; λ denotes a tapered parameter related to the tree species.

The cross-sectional area of the branch is defined as follows

$$A_b = \pi r_b^2 \quad (8)$$

where r_b denotes the cross-sectional radius of a branch.

The parameters of the primary branches are given in Table 1. The cross-sectional radius of a secondary branch is assumed to be 0.005 m. The ratio of the length of the secondary branch and its corresponding primary branch is 0.2. The tapered parameter of the trunk is valued by 0.6 in this study through the investigation of *Ginkgo* trees in the local area.

3.2 Finite element modelling

Since the bending plays a significant role revealing the behaviors of trees, a three-dimensional beam element with a circular cross section is used to model the urban tree. The axis of the beam element is defined according to the tangent at the same location of the geometric model. The commonly used MATLAB-language routine is coded to artificially mesh the geometric model of urban trees, whereby the ABAQUS input file is generated. The trunk is divided into 20 elements; each component of the primary branches is divided into 10 elements; and each component of the secondary branches is divided into 5 elements.

In accordance with previous work (Sellier *et al.* 2006, 2008), the material of the tree is assumed to be isotropic and homogeneous. The density and the Young's Modulus of the tree are valued by 472 kg/m^3 and 0.99 GPa, respectively, according to the Chinese Wood Handbook (Cheng *et al.* 1992). The Poisson's ratio is denoted by 0.38 (Sellier *et al.* 2006).

A nonlinear material constitutive law showing elastic-plastic behavior with isotropic hardening is used herein. This elastic-plastic model is defined through the data assimilation of the stress-plastic strain pairs referring to the Chinese Wood Handbook (Cheng *et al.* 1992) where three mechanical stages are exposed, i.e., linear-elastic stage, nonlinear-plastic stage and rupture.

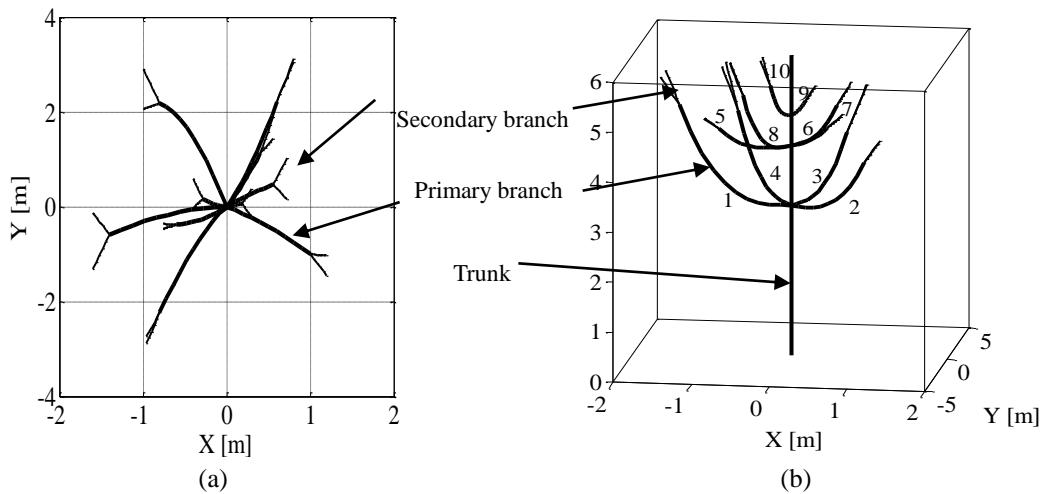


Fig. 2 Model of Ginkgo tree: (a) plan view and (b) geometry of a synthetic tree

Table 1 Geometric parameters of primary branches*

Number of the branches	Values of Radius	Arc Length
1st	0.020 m	2.766 m
2nd	0.020 m	1.886 m
3rd	0.020 m	2.677 m
4th	0.020 m	3.236 m
5 th	0.015 m	2.492 m
6 th	0.015 m	1.117 m
7 th	0.015 m	1.224 m
8 th	0.015 m	1.467 m
9 th	0.010 m	0.349 m
10 th	0.010 m	0.702 m

*The branches spreading at the same height from the trunk is assumed to be a same radius. The 1st-4th, 5th-8th and 9th, 10th primary branches extends at a height of 3 m, 4.2 m, 4.8 m respectively (see Fig. 2)

As shown in Fig. 3, the yield point is 22.4 MPa at 0.26% compressive strain and the ultimate strength is 39.2 MPa at 0.8% compressive strain. For reference purpose, the material constitutive laws proposed by Brudi upon the two different tree species are shown in the figure. The elastic-plastic model used in this study exhibits a same yield strain with the Brudi's models, while the former occupies a larger Young's modulus due to statistics of urban tree specimens in Chinese Wood Handbook.

Regarding to the boundary condition of the finite element model, as shown in Fig. 2, the numerical tree is clamped at its base, and rotation is fixed at each branching point (this boundary condition is necessary for the branching points to support moments). This model is asymmetrical and close to the real configuration of a *Ginkgo* tree. The fundamental nature frequency of the modelled *Ginkgo* tree is round 1.1 Hz, which shows an agreement with the on-site testing results investigated by Baker (Baker 1997).

3.3 Wind loading

The logical definition of wind loading upon a tree is a challenging issue due to the complexity inherent in the flow and turbulence structures around the tree (Aly *et al.* 2013, Lee *et al.* 2014). In this paper, the interaction between the wind and the tree is treated as a wind drag force (Ciftci *et al.* 2014), which is modelled as a distributed line loads acting on the finite element model in x direction (all loadings are applied in a horizontal direction). The drag force acting on the j -th element of the model is expressed as

$$F_j(t) = 0.5\rho_a A_j(t)C_D U_j^2(t) \quad (9)$$

where $U_j(t)$ denotes the velocity of wind distributing on the j -th element; $A_j(t)$ denotes the project area of the j -th element ($j = 1, 2, \dots, N_e$), where N_e denotes the number of the elements; ρ_a denotes the density of air; C_D is the drag coefficient. The density of air and the drag coefficient are assumed to be 1.2 kg/m^3 and 0.47, respectively (Rudnicki *et al.* 2004).

4. Dynamic analysis of Ginkgo trees

Based on the D'Alemberts principle and the finite element method (Zienkiewicz 1991), the dynamic response of j -th element of the model subjected to wind loading reads

$$\mathbf{M}_j \ddot{\mathbf{u}}_j(t) + \mathbf{C}_j \dot{\mathbf{u}}_j(t) + \mathbf{f}[\mathbf{u}_j(t)] = \mathbf{F}_j(t) \quad (10)$$

where \mathbf{M}_j and \mathbf{C}_j ($j=1,2,\dots,N_e$) denote the mass and damping matrices of the j -th element, respectively. $\ddot{\mathbf{u}}_j(t)$, $\dot{\mathbf{u}}_j(t)$, $\mathbf{u}_j(t)$ denote vectors of the acceleration, velocity, and displacement of the tree with respect to ground, respectively. $\mathbf{f}[\mathbf{u}_j(t)]$ denotes a vector of internal restoring forces of the j -th element, serving as a function of the elemental deflections. $\mathbf{F}_j(t)$ denotes the time-dependent load vector of the j -th element. Rayleigh damping is used here to approximate the damping matrix $\mathbf{C}_j = k_1 \mathbf{M}_j + k_2 \mathbf{K}_j$, where k_1 and k_2 are Rayleigh damping factors, respectively. It is assumed herein that k_1 is valued by 0.32 and k_2 is valued by 0.001 (Sellier *et al.* 2006). The motion of trees subjected to wind actions involves geometric nonlinearity and material nonlinearity, of which the nonlinear effect is included in the term of restoring forces $\mathbf{f}[\mathbf{u}_j(t)]$.

It should be noted that the effect of geometric nonlinearity in the analysis would be considered in case that the NLGEOM parameter in the step definition is defined as YES. The analysis is undertaken using a scheme of Hilber-Hughes-Taylor time integration with default settings in Abaqus/Standard (Version 6.10, Hibbitt, Karlsson & Sorensen, Inc. USA). The parameters α , β , λ corresponding to the transient fidelity are denoted by -0.05 , 0.275625 and 0.55 , respectively; while they are denoted by -0.41421 , 0.5 and 0.91421 , respectively, corresponding to moderate dissipation.

4.1 Dynamic response of the Ginkgo tree subjected to wind loading

The dynamic analysis is performed for a total period of 600 seconds with assumption of the stationary initial conditions. The response process of the top displacement and the maximum bending moment (along all the structural components which typically occurs at the bottom of the trunk) are plotted as a function of time. Fig. 4 shows the time history of top displacement and maximum bending moment in case of mean wind velocity 24 m/s. It can be seen that the top displacement and maximum bending moment oscillates with time and follows the trend of the wind action. It is also found that the response solution derived from linear and nonlinear analysis meets closely with each other at the initial un-yield stage of *Ginkgo* trees. However, the significant difference between the nonlinear and the linear analysis occurs when the structural component locates at nonlinear-plastic stage, where the large deformation arises on the *Ginkgo* tree resulting in a lower bending moment due to the elastic-plastic material constitutive law used in the nonlinear analysis of the structural model. It is indicated that the nonlinearities inherent in the *Ginkgo* tree (coupling the material and geometric nonlinearities) affect its dynamic behaviors seriously.

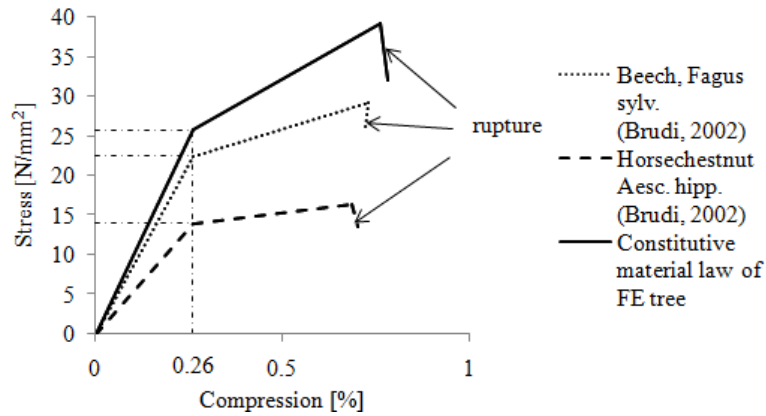


Fig. 3 Constitutive material law of trees

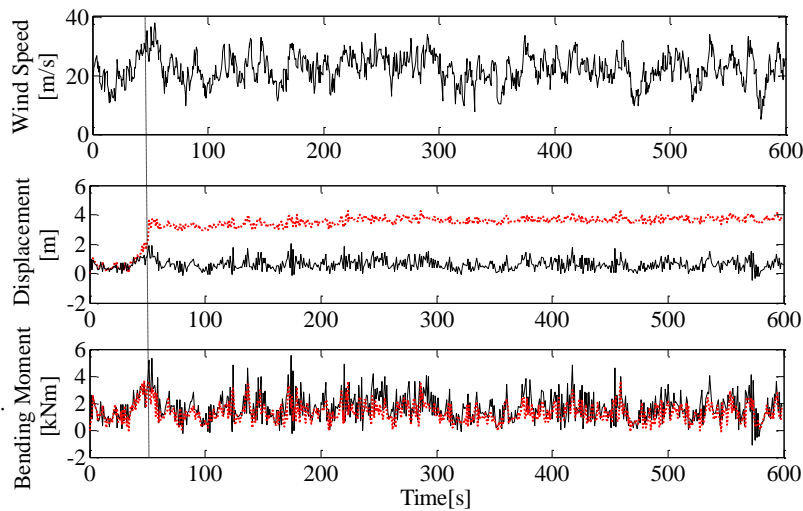


Fig. 4 Time history of top displacement and maximum bending moment at mean wind velocity of 24 m/s, with a comparison of the nonlinear analysis (dashline) and linear analysis (solid line)

Phase portraits of top displacement of the structural model derived from the nonlinear analysis corresponding to typical mean wind velocities are shown in Fig. 5. In accordance with the time history of top displacement in case of mean wind velocity 24 m/s, the phase portrait; see Fig. 5(b), reveals that at the first period the *Ginkgo* tree locates at a non-stationary state owing to damping influence of the structural system, it jumps to a stationary state moving back and forward where the tree features a plastic behavior. A sounder phase shifting phenomenon exposes in case of mean wind velocity 32 m/s; see Fig. 5(c). While in case of lower amplitude of the wind action, e.g., with mean wind velocity 12 m/s; see Fig. 5(a), the *Ginkgo* tree still features an elastic behavior and gives rise to a small-range oscillation.

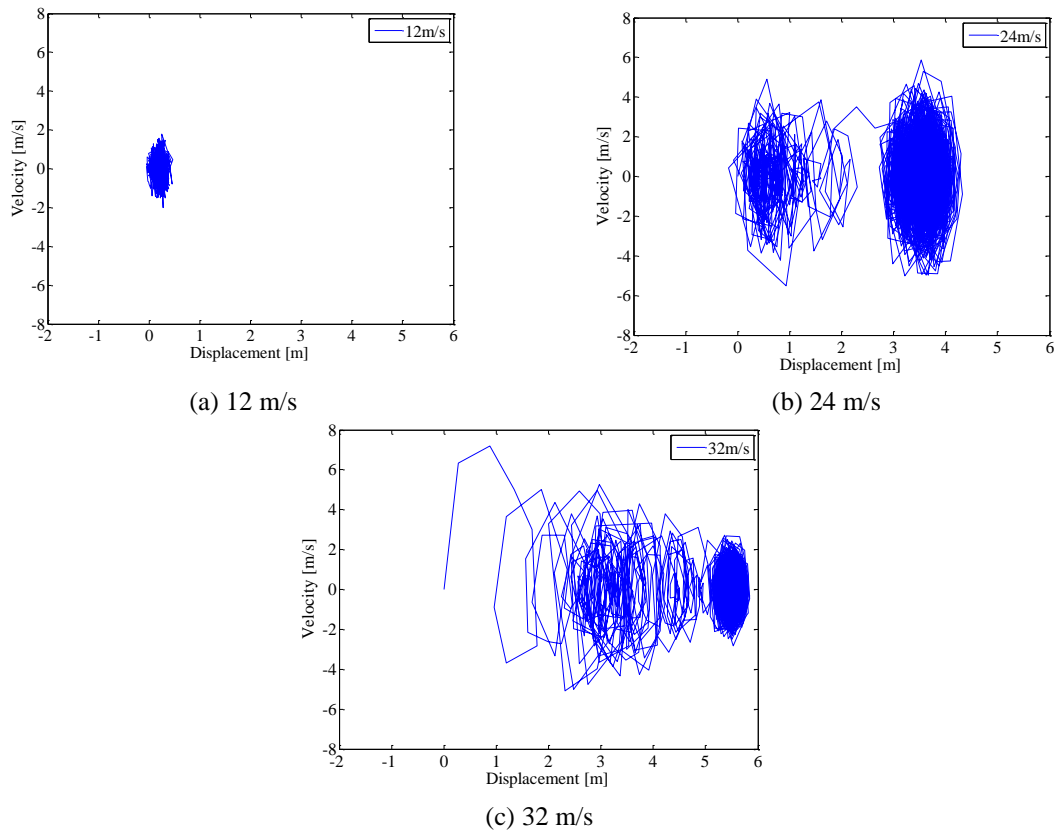


Fig. 5 Phase portraits of top displacement derived from the nonlinear analysis corresponding to different mean wind velocity of (a) 12 m/s, (b) 24 m/s and (c) 32 m/s, respectively

Fig. 6 shows the contour plots of bending moment at the instant of maximum value derived from the nonlinear analysis corresponding to typical mean wind velocities. It is seen that in case of mean wind velocity 12 m/s, the range of bending moment is $[-49, 1000]$ Nm. While the range will be extended along with the increase of wind velocity; see Figs. 6(b) and 6(c), the range of bending moment is $[-170, 4000]$ Nm and $[-140, 4100]$ Nm in case of mean wind velocity 24 m/s and 32 m/s.

4.2 Nonlinearity effects of dynamic response

In order to reveal the nonlinearity effects of dynamic response with relevance to the external excitation, the responses of *Ginkgo* tree subject to wind actions in different magnitude levels are investigated. Fig. 7 shows a comparison of the maximum bending moment obtained from the nonlinear analysis and linear analysis at the mean wind velocity 12 m/s, 24 m/s and 32 m/s, respectively. It is seen that the result of the mean wind velocity at 12 m/s calculated in the nonlinear analysis matches the linear analysis result well; see Fig. 7(a).

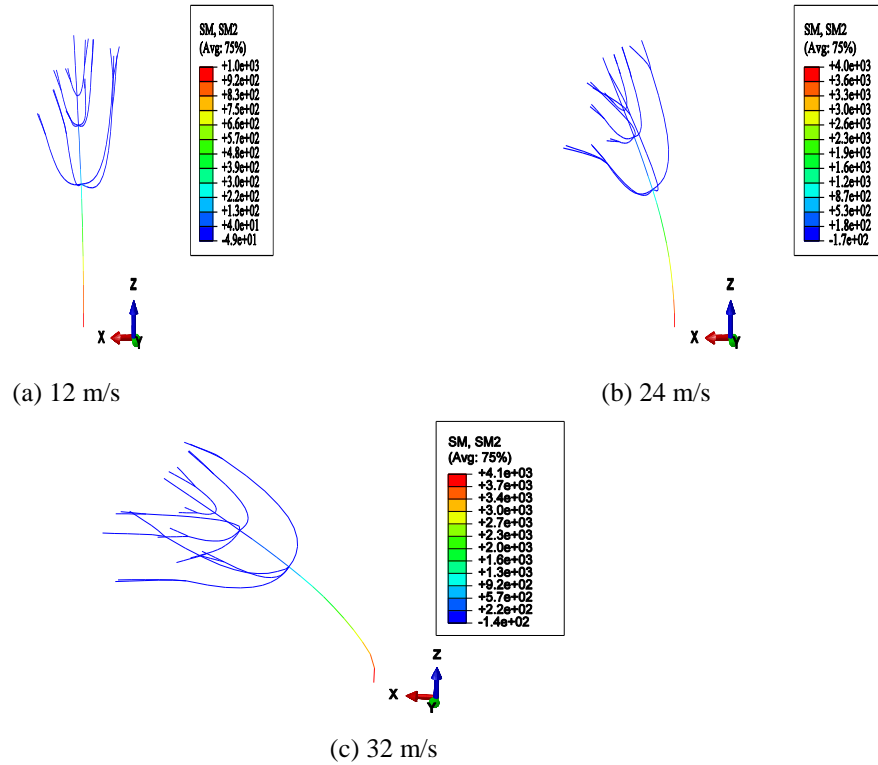


Fig. 6 Contour plots of bending moment at instant of maximum value derived from the nonlinear analysis corresponding to different mean wind velocity of (a) 12 m/s, (b) 24 m/s and (c) 32 m/s, respectively

This exposes that the nonlinearity inherent in the structural dynamics has no significant effect on the maximum bending moment in case of the mean wind velocity less than 12 m/s, indicating that the dynamic behavior of the *Ginkgo* tree subjected to wind actions satisfies the ‘small deformation hypothesis’. Still, in the case of mean wind velocity 24 m/s, the maximum bending moments obtained from nonlinear analysis and linear analysis obviously split at a time instant. It shows the nonlinearity begins to influence the motion of the *Ginkgo* tree, where the response magnitude in case of the nonlinear analysis is relatively smaller than that of the linear analysis. It is explained that a compensative moment is provided by the axial deflection of structural components due to geometric nonlinearity and a reduced response moment is produced by the yield stress of structural components due to material nonlinearity, which results in a lower resistant bending moment. When the mean wind velocity reaches to 32 m/s, the splitting time instant between the maximum bending moment calculated from the nonlinear analysis and from the linear analysis shifts to an earlier as the mean wind velocity 24 m/s. Meanwhile, the response of the maximum bending moment calculated by nonlinear analysis is large initially and rapidly approaches to zero, indicating that the *Ginkgo* tree enters into rupture and a hinge occurs at the bottom of the trunk. The rupture state that the *Ginkgo* tree locates at could be also explained in the following analysis of top displacement of structural model.

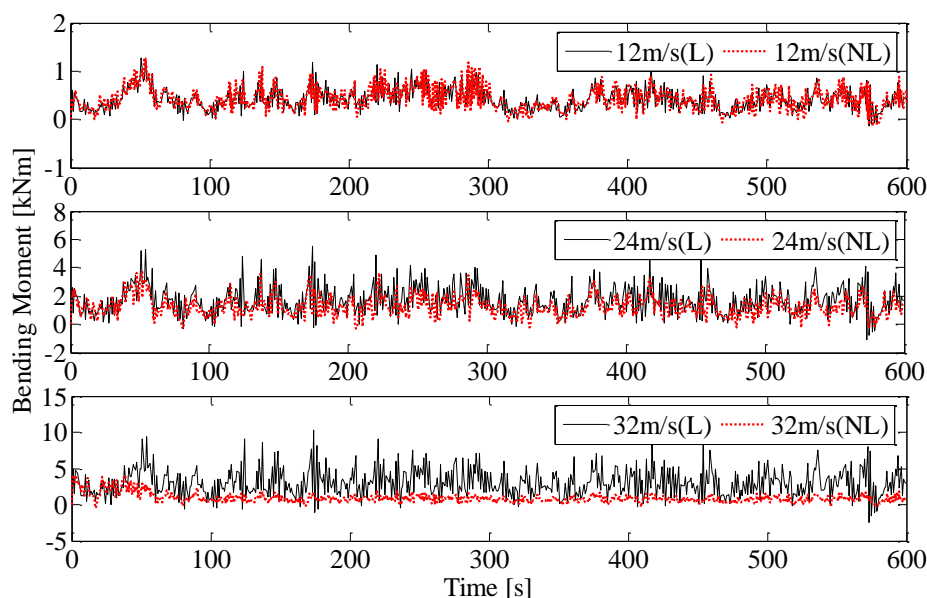


Fig. 7 Time history of maximum moment between the nonlinear analysis (dotted line) and linear analysis (solid line) at mean wind velocity of 12 m/s, 24 m/s and 32 m/s, respectively

The similar characteristics are included in Fig. 8 by exploring the time history of top displacement obtained from the nonlinear analysis and linear analysis, respectively. At the mean wind velocity 12 m/s, the top displacement processes fairly consistent with each other indicating that the tree has been in the elastic range. At the mean wind velocity 24 m/s, however, the top displacement of the tree jumps to a larger amplitude due to the static wind action after an initial period indicating that the *Ginkgo* tree reaches to the plastic range and cannot go back to its initial position. Whilst the linear analysis shows the oscillation of the tree dragged by wind. The oscillation can also be found in the linear analysis at the mean wind velocity 32 m/s in contrast to the nonlinear case, which shows that the *Ginkgo* tree fails, e.g., the top displacement close to 6m (model's height).

Fig. 9 shows the extreme value of the maximum bending moment plotted against the wind velocity, comparing the linear analysis and nonlinear analysis. It is found that along with the increase of wind velocity, the nonlinearity effect of dynamic response of *Ginkgo* tree arises to be significant, which is sound in case that the mean wind velocity goes beyond 20 m/s.

It is explained that the bending moment acts as an integral of the stress distributed in the cross-section (Beer *et al.* 2012); if the stress reaches its ultimate strength they would not increase more. Since the stress of the cross-section in case of the mean wind velocity beyond 20 m/s closes to its ultimate value during the nonlinear analysis, the resistant bending moment thus approaches to its maximum value and cannot increase much further. The extreme value of the maximum top displacement plotted against the wind velocity is shown in Fig. 10.

As remarked previously, the top displacement of nonlinear analysis enhances significantly against that of linear analysis with the increase of wind velocity due to the usage of the nonlinear material constitutive law.

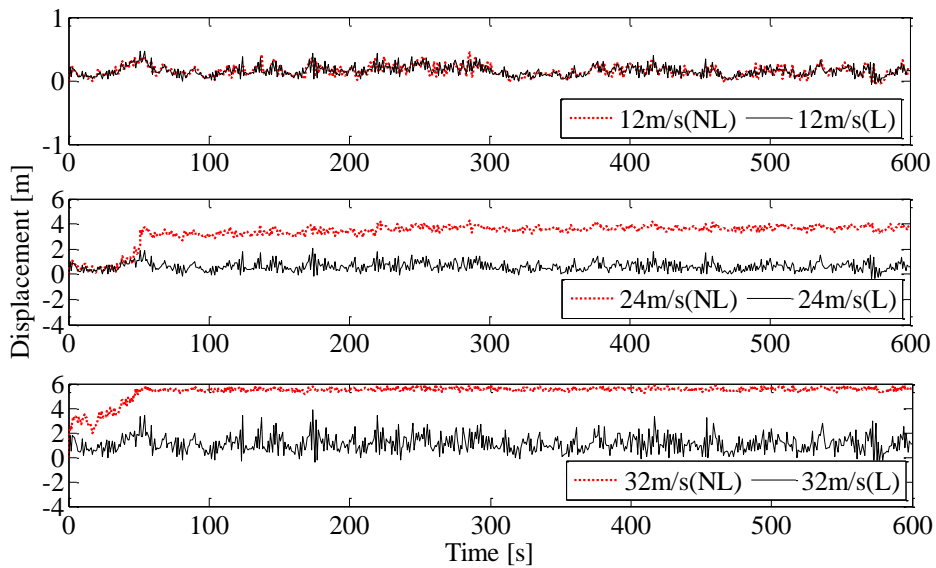


Fig. 8 Time history of top displacement between the nonlinear analysis (dotted line) and linear analysis (solid line) at wind velocity of 12 m/s, 24 m/s and 32 m/s, respectively

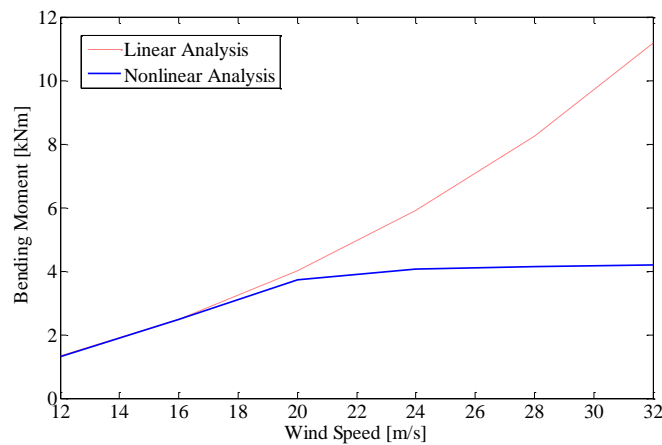


Fig. 9 Comparison of the extreme value of maximum bending moment against the wind velocity between the linear analysis (dash line) and the nonlinear analysis(solid line)

5. Failure analysis of Ginkgo trees

It is clearly indicated in the previous section that the *Ginkgo* tree model ruptures when the bending moment exceeds its failure bending moment. In this case, the response of maximum bending moment turns to be zero and value of the top displacement is close to the tree's height. All

these findings show that the nonlinear analysis more accurately exhibits the failure phenomenon of *Ginkgo* trees.

The purpose of this study is to assess the risk of *Ginkgo* tree failure. The bending moment is a critical parameter to determine whether the tree is failure or not. Failure of a *Ginkgo* tree during a time period is defined as the state of a spatial element where the maximum value of wind-induced bending moment first exceeds its resistant moment, i.e., the capacity of trunk or branches resisting failure. The resistant moment in this case is so-called the failure moment. Arising from theory of bending, the failure moment is given by (Beer *et al.* 2012)

$$\hat{B}_j = \frac{\sigma \pi r_j^3}{4} \quad (11)$$

where \hat{B}_j is the failure moment of the j -th element, $j=1,2,\dots,N_e$; σ is the resistance of the material of green wood; r_j is the radius of the j -th element. The wind velocity at which the maximum value of the tree response moment is equal to its failure moment is termed the ‘failure wind velocity’.

The state of j -th element can be defined as the following index

$$I_j = H[\max_{t \in [0,T]} \{ |B_j(t)| \} - \hat{B}_j] \quad (12)$$

where I_j denotes the state of the element: $I_j = 0$ indicating a safe element, $I_j = 1$ indicating a failure element; \hat{B}_j denotes the threshold of element safety, and here it is the failure bending moment; $B_j(t)$ denotes the time-dependent response moment; $H[\cdot]$ denotes a Heaviside function.

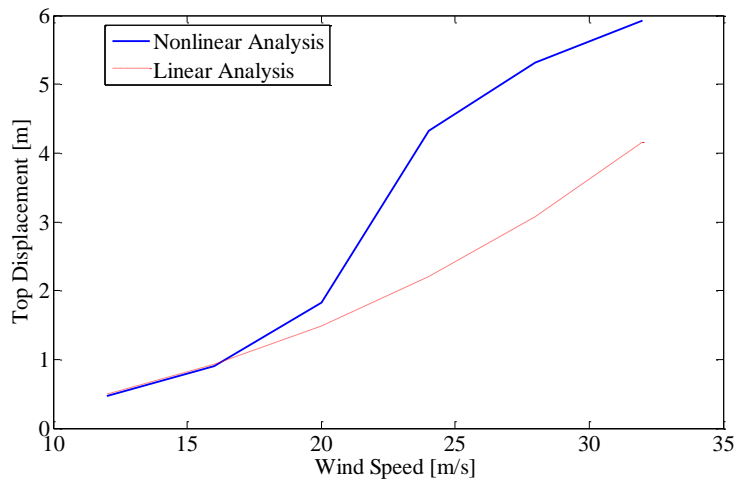


Fig. 10 Comparison of extreme value of top displacement against the wind velocity between the linear analysis (dash line) and the nonlinear analysis (solid line)

The failure percentage is an index representing the ratio between failure elements and total elements of a certain structural layer such as the trunk, primary branches or secondary branches

$$P_{f,i} = \frac{\sum_{j=1}^{N_i} I_j}{N_i} \quad (13)$$

in which $P_{f,i}$ is the failure percentage of i -th structural layer; N_i ($i=1,2,3$) denotes the element number of a certain structural layer.

The failure wind velocity is identified using the scheme of nonlinear analysis. Fig. 11 shows the envelopes of maximum bending moments along the trunk at different mean wind velocity of 12 m/s, 16 m/s, 20 m/s, 24 m/s, 28 m/s and 32 m/s, respectively. It is suggested that for cases of each wind velocity the maximum value of the bending moment occurs at the bottom of the *Ginkgo* tree. The maximum bending moment increases with the enhancement of the wind velocity, while does not increase much further when the wind velocity exceeds 24 m/s due to the effect of material nonlinearity. The failure moment of spatial elements of the trunk along its height is exposed in Fig. 11 as well. It is seen that the failure moment is always larger than the maximum value of the tree response moment along with the trunk in case of mean wind velocity not more than 20 m/s. From Fig. 11, the failure wind velocity of trunk corresponding to its failure moment is 24 m/s for this case using interval of wind velocity 4 m/s. Moreover, a sudden decreasing at 3 m height and a sudden increasing slope at 3.3 m height are found in the figure as well. The reason of a sudden decreasing at 3 m height is that at this height the branches share the bending moment carried by the trunk, where the four primary branches are involved. The sudden increasing slope at 3.3 m height is owing to the usage of finite element method that the trunk is equally divided 20 elements and the bending moment slope will give rise at the other node of the element. It is understood that the more the elements used in the trunk, the shorter the distance between the sudden decreasing point and sudden increasing slope point would be.

There is a fact that the branches failure occurs earlier than the trunk failure with the increase of mean wind velocity. As indicated in Section 3, the trunk, primary branches and secondary branches involves 20, 100 and 100 elements, respectively. For the trunk elements, they consist of a serial system with independent element failure, indicating that the trunk would fail once any of the trunk elements is failure. While for the primary branches, they consist of a parallel system with conditionally independent element failure. The conditional failure is understood as the fact that if the trunk fails the primary branches are all failure. The parallel system happens to be failure only in case that all the primary branches fail. Similarly, the secondary branches consist of a parallel system with conditionally independent element failure. The conditional failure links to the fact that a group consisting of several secondary branches would fail if the group hinges upon one failure primary branch. The parallel system thus happens to fail only in case that all the secondary branches fail. Fig. 12 presents the failure percentage of the *Ginkgo* tree model under different mean wind velocities, where the logical relationship among the trunk, primary branches and secondary branches is included. It is seen that all the elements at the three structural layers of tree is more vulnerable to failure with an increase of wind velocity. Differences between samples from the same species or from the different species would result in a significant variation of failure percentage since the frontal area, moment capacity and drag force link with the structural configurations, wood properties and living conditions. The importance of these differences is addressed in the previous studies (Ciftci *et al.* 2014).

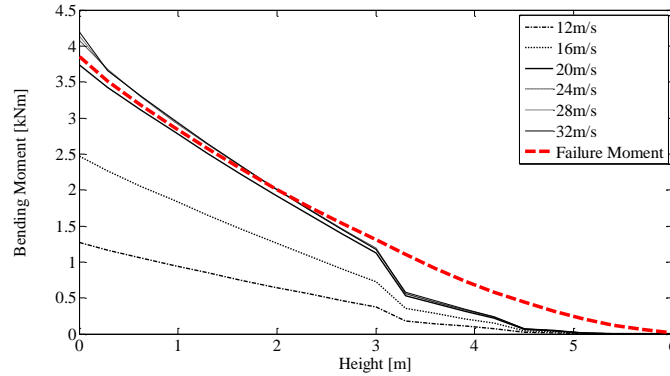


Fig. 11 Envelopes of the maximum bending moments along the Ginkgo trunk corresponds to different wind velocity of 12 m/s, 16 m/s, 20m/s, 24 m/s, 28 m/s and 32 m/s, respectively

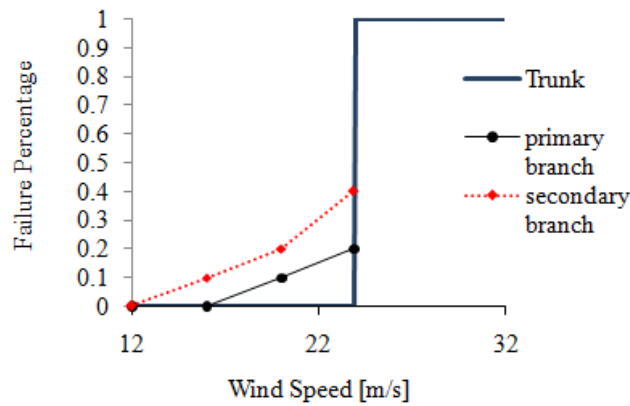


Fig. 12 Failure percentage of Ginkgo tree model under different mean wind velocities of 12 m/s, 16 m/s, 20 m/s, 24 m/s, 28 m/s and 32 m/s, respectively

It is also found that the secondary branches are more likely to fail than the primary branches, where a non-proportional failure percentage among them is exposed. There are two physical quantities controlling the failure of the tree branches. One is the moment capacity of the branch, and the other is the wind-induced branch bending moment. In this study, the moment capacity of the branch hinges upon the resistance of green wood material and the radius of branch (see Eq. (11)). The secondary branches have a smaller cross sectional radius than the primary branches, where the ratios between cross sectional radius of the latter and of the former at the three heights are 4, 3, 2, respectively. Consequently, the ratios between moment capacity of the latter and of the former at the three heights are 64, 27, 8, respectively. While the wind-induced bending moment of the latter is just 4 times than the former at the same height. It is thus explained that secondary branches are more likely to fail for this case.

6. Conclusions

In this paper we have focused on wind damage to *Ginkgo* trees via the numerical solution techniques. The contribution of this paper lies in introducing a more accurate method to assess the likelihood of *Ginkgo* tree expected to fail under wind action through coupling the effects of geometric nonlinearity and material nonlinearity. The concept of the failure wind velocity is also proposed to assess the vulnerability of *Ginkgo* trees. Some concluding remarks are included as follows:

- (1) The coupling effects of the material and geometric nonlinearities affect the dynamic behaviors of trees seriously. A larger deformation and a lower bending moment are exposed in the nonlinear analysis due to the elastic-plastic material constitutive law used in the structural model.
- (2) The failure moment is always larger than the maximum value of the tree response moment along with the height of trunk in case of mean wind velocity not more than 20 m/s. The failure wind velocity of trunk, in the present case, corresponding to its failure moment is 24 m/s.
- (3) The trunk elements consist of a serial system with independent element failure, while the primary and secondary branches consist of a parallel system with conditionally independent element failure, respectively. The failure pattern of the structural elements highly relies upon the topology of trees.

It should be noted that the dynamic behavior varies with the type of trees, the season and trees' age etc. (Baker 1997, James *et al.* 2006, Ciftci *et al.* 2014). The failure wind velocity predicted by previous studies thus shifts from 17m/s (Oliver and Mayhead 1974) to 35m/s (Cucchi *et al.* 2005). Further development of this study could implement a statistical analysis and reliability assessment of wind-induced damage of trees to examine the uncertainty effects derived from the structural properties and external excitations.

Acknowledgements

The supports of State Key Laboratory of Disaster Reduction in Civil Engineering at Tongji University (Grant Nos. SLDRCE13-MB-04, SLDRCE14-B-20) and Project of National Key Technology R&D Program in the 12th Five Year Plan of China (2012BAJ11B01) are highly appreciated. The authors also thank Prof. Jie Li for his constructive suggestions and consistent supports on the researches.

References

- Aly, M.A., Fabio, F. and Sara, M. *et al.* (2013), "Wind loading on trees integrated with a building envelope", *Wind Struct.*, **17**(1), 69-85.
- Baker, C.J. (1995), "The development of a theoretical model for the windthrow of plants", *J. Theor. Biol.*, **175**, 355-372.
- Baker, C.J. (1997), "Measurements of the natural frequencies of trees", *J. Exper. Botany*, **48**(310), 1125-1132.
- Beer, F.P., Johnston, E.R., DeWolf, J.T. and Mazurek, D.F. (2012), *Mechanics of Materials*, McGraw-Hill, New York, United States.

- Brudi, E. (2002), *Trees and Statics: An introduction*. Arborist News: 28-33.
- Cheng, J.Q., Yang, J.J. and Liu, P. (1992), *Chinese Wood Handbook*, Chinese Forestry Press, Beijing, China, (in Chinese).
- Ciftci, C., Arwade, S.R., Kane, B. and Brena, S.F. (2014), "Analysis of the probability of failure for open-grown trees during wind storms", *Probabilist. Eng. Mech.*, **37**, 41-50.
- Ciftci, C., Brena, S.F., Kane, B. and Arwade, S.R. (2013), "The effect of crown architecture on dynamic amplification factor of an open-grown sugar maple (*Acer saccharum* L.)", *Trees*, **27**, 1175-1189.
- Cucchi, V., Meredieu, C., Stokes, A., DeColigny, F., Suarez, J. and Gardiner, B., (2005), "Modelling the windthrow risk for simulated forest stands of Maritime pine (*Pinus pinaster* Ait.)", *Forest Ecol. Manag.*, **213**, 184-196.
- Dahle, G.A. and Grabosky, J.C. (2010), "Variation in modulus of elasticity (E) along *Acer platanoides* L.(Aceraceae) branches", *Urban Forestry & Urban Greening*, **9**, 227-233.
- Davenport, A.G. (1961), "The spectrum of horizontal gustiness near the ground in high winds", *Q. J. Roy. Meteorol. Soc.*, **87**(372), 194-211.
- Dyrbye, C. and Hansen, S.O. (1997), *Wind Loads on Structures*, John Wiley and Sons, Chichester, England.
- Gardiner, B.A., Peltola, H. and Kellomaki, S. (2000), "Comparison of two models for predicting the critical wind velocities required to damage coniferous trees", *Ecol. Model.*, **129**(1), 1-23.
- James, K.R., Haritos, N. and Ades, P.K. (2006), "Mechanical stability of trees under dynamic loads", *Am. J. Botany*, **93**(10), 1522-1530.
- Jim, C.Y. and Liu, H.T. (1997), *Storm damage on urban trees in Guangzhou*, China. *Landscape and Urban Planning*, **38**, 45-59.
- Kareem, A. (2008), "Numerical simulation of wind effects: a probabilistic perspective", *J. Wind Eng. Ind. Aerod.*, **96**(10-11), 1472-1497.
- Lee, J.P., Lee, E.J. and Lee, S.J. (2014), "Effect of trunk length on the flow around a fir tree", *Wind Struct.*, **18**(1), 69-82.
- Lipecki, T. and Flaga, A. (2010), "Direct simulation of vortex excitation by using stochastic methods", *Proceedings of the 5th International Symposium on Computational Wind Engineering (CWE2010) Chapel Hill, North Carolina, USA May 23-27*.
- Oliver, H.R. and Mayhead, G.J. (1974), "Wind measurements in a pine forest during a destructive gale", *Forestry*, **47**(2), 185-194.
- Rossi, R., Lazzari, M. and Vitaliani, R. (2004), "Wind field simulation for structural engineering purposes", *Int. J. Numer. Meth. Eng.*, **61**(5), 738-763.
- Rudnicki, M.R., Mitchell, S.J. and Novak, M.D. (2004), "Wind tunnel measurements of crown streamlining and drag relationships for three conifer species", *Can. J. Forest Res.*, **34**(3), 666-676.
- Saunderson, S.E.T., Baker, C.J. and England, A. (1999), "A dynamic model of the behaviour of Sitka Spruce in high winds", *J. Theor. Biol.*, **200**(3), 249-259.
- Sellier, D., Fourcaud, T. and Lac, P. (2006), "A finite element model for investigating effects of aerial architecture on tree oscillations", *Tree Physiol.*, **26**(6), 799-806.
- Sellier, D., Brunet, Y. and Fourcaud, T. (2008), "A numerical model of tree aerodynamic response to a turbulent airflow", *Forestry*, **81**(3), 279-297.
- Simiu, E. (1974), "Wind spectra and dynamic along wind response", *J. Struct. Division*, **100**(9), 1897-1910.
- Spatz, H.C.H. and Bruechert, F. (2000), "Basic biomechanics of self-supporting plants: wind loads and gravitational loads on a Norway spruce tree", *Forest Ecol. Manag.*, **135**(2000), 33-44.
- Spatz, H.C.H. and Speck, O. (2002), "Oscillation frequencies of tapered plant stems", *Am. J. Botany*, **89**(1), 1-11.
- Zienkiewicz, O.C. and Taylor, R.L. (1991), *The finite element method*, 4th Ed., Mc.Graw-Hill, London.